



# Geochemistry, Geophysics, Geosystems

## RESEARCH ARTICLE

10.1029/2019GC008418

### Special Section: Polar region geosystems

#### Key Points:

- First heat flow measurements from the Coompana Province, southern Australia, indicate values of  $40\text{--}70\text{ mW/m}^2$  ( $57 \pm 3\text{ mW/m}^2$  average)
- A tectonically reconstructed heat flow map constrains the thermal regime of geological provinces formerly contiguous with East Antarctica
- Geophysical models of Antarctic heat flow are likely underestimating crustal sources of radiogenic heat that influence subglacial melting

#### Supporting Information:

- Supporting Information S1
- Table S1
- Table S2

#### Correspondence to:

A. Pollett,  
alicia.pollett@unisa.edu.au

#### Citation:

Pollett, A., Hasterok, D., Raimondo, T., Halpin, J. A., Hand, M., Bendall, B., & McLaren, S. (2019). Heat flow in Southern Australia and connections with East Antarctica. *Geochemistry, Geophysics, Geosystems*, 20, 5352–5370. <https://doi.org/10.1029/2019GC008418>

Received 29 APR 2019

Accepted 26 SEP 2019

Accepted article online 23 OCT 2019

Published online 27 NOV 2019

## Heat Flow in Southern Australia and Connections With East Antarctica

Alicia Pollett<sup>1</sup> , Derrick Hasterok<sup>2</sup>, Tom Raimondo<sup>1,3</sup> , Jacqueline A. Halpin<sup>4</sup> , Martin Hand<sup>2</sup>, Betina Bendall<sup>5</sup>, and Sandra McLaren<sup>6</sup>

<sup>1</sup>School of Natural and Built Environments, University of South Australia, Adelaide, South Australia, Australia, <sup>2</sup>Geology and Geophysics, School of Physical Sciences, University of Adelaide, Adelaide, South Australia, Australia, <sup>3</sup>Future Industries Institute, University of South Australia, Adelaide, South Australia, Australia, <sup>4</sup>Institute for Marine and Antarctic Studies, University of Tasmania, Hobart, Tasmania, Australia, <sup>5</sup>Energy Resources Division, South Australian Department for Energy and Mining, Adelaide, Australia, <sup>6</sup>School of Earth Sciences, University of Melbourne, Melbourne, Victoria, Australia

**Abstract** Viscosity and melt generation at the base of ice sheets are critically dependent upon heat flow. Yet subglacial heat flow is poorly constrained due to the logistical challenges of obtaining boreholes that intersect the bedrock beneath thick ice cover. Currently, continental estimates of Antarctic heat flow are derived from geophysical methods that provide ambiguous constraints of crustal heat sources, despite their demonstrated importance for accurate predictions of future ice sheet behavior. This study pursues an alternative approach by using heat flow measurements from rock units in the Coompana Province of southern Australia, which represent the geological counterparts of those beneath Wilkes Land in East Antarctica. We present nine new surface heat flow estimates from this previously uncharacterized region, ranging from  $40$  to  $70\text{ mW/m}^2$  with an average of  $57 \pm 3\text{ mW/m}^2$ . These values compare favorably to recent geophysically derived estimates of  $50\text{--}75\text{ mW/m}^2$  for the Totten Glacier catchment of East Antarctica, and to the single in situ measurement of  $75\text{ mW/m}^2$  from the Law Dome deep ice borehole. However, they are appreciably lower than the range of  $56\text{--}120\text{ mW/m}^2$  ( $83 \pm 13\text{ mW/m}^2$  average) for the abnormally enriched Proterozoic terranes of the Central Australian Heat Flow Province. This study provides the first regional heat flow map of geological provinces formerly contiguous with East Antarctica through the application of continent-scale heat flow data sets tied to a Jurassic plate tectonic reconstruction for Gondwana. Our approach reveals several discrepancies with current heat flow models derived from geophysical methods and provides a more robust analysis of subglacial heat flow using this plate tectonic synthesis as a proxy for East Antarctica.

**Plain Language Summary** The Antarctic ice sheet currently represents the largest source for potential sea level rise. Understanding Antarctic ice sheet behavior is important for predicting ice sheet movement and possible melting. Heat that flows from the crust to the base of the ice sheet is a significant contributor to ice sheet behavior. Obtaining estimates of heat flow across Antarctica are problematic due to the logistical challenges of accessing bedrock that lies beneath thick ice cover. Consequently, thermal conditions are currently estimated using geophysical data, from which temperatures beneath the ice extending into the crust and mantle are derived. However, large discrepancies exist between alternative geophysical models, and there remains the need to validate these models and assess their accuracy. This study takes a new approach by using heat flow estimates from southern Australia as a proxy for heat flow in East Antarctica. Plate tectonic reconstructions indicate that approximately 160 million years ago, Australia and East Antarctica were conjoined. We argue that the rocks and corresponding heat flow values of southern Australia are genuine counterparts to those beneath the ice in East Antarctica. If true, this suggests that existing geophysical models can be tested against our reconstructed heat flow maps of this shared tectonic margin.

## 1. Introduction

Numerous studies suggest that the Antarctic ice sheet will be a significant contributor to future sea level rise (DeConto & Pollard, 2016; Overpeck et al., 2006; Pritchard et al., 2012; Rignot et al., 2011). Geothermal heat flow is a critical factor controlling temperature conditions at the base of the ice sheet, and consequently plays a fundamental role in current and future ice sheet movement (Schroeder et al., 2014; Tulaczyk et al., 2000; Winsborrow et al., 2010). However, subglacial heat flow in Antarctica is poorly constrained due to lack of accessibility, a direct consequence of the logistical challenges of drilling through ice that is on average up to 2 km thick (Fretwell et al., 2013) to intercept the bedrock that lies beneath.

Heat flow is the output of the combined heat produced from the convective mantle and the radiogenic heat production of the lithosphere (in practice largely from the crust). In Antarctica, it constitutes a major control on basal temperature (the temperature at the interface between the base of the ice sheet and underlying bedrock), a parameter without which ice sheet behavior cannot be modeled (Pittard et al., 2016; Seroussi, Morlighem, et al., 2017; Simkins et al., 2017; Szuman et al., 2018). A study by Llubes et al. (2006) demonstrates that a change in heat flow from 40 to 60 mW/m<sup>2</sup> results in basal temperatures increasing by a few degrees Celsius at the East Antarctic coastline, to 15 °C in the East Antarctic interior. This plainly demonstrates the necessity for accurate modeling (and measurement, where possible) of heat flow across the Antarctic continent, in order to robustly calculate the resulting basal temperatures and constrain the basal conditions that determine ice movement.

Current models of Antarctic subglacial heat flow are derived from satellite and airborne magnetic and ground-sourced seismic data, which allow for the derivation of geothermal gradients using Curie depth temperature isotherms (Martos et al., 2017) and upper mantle seismic velocity (An et al., 2015). In East Antarctica, these models yield mean estimates of approximately 50–60 mW/m<sup>2</sup> (An et al., 2015; Fox Maule et al., 2005; Martos et al., 2017; Shapiro & Ritzwoller, 2004; Van Liefferinge & Pattyn, 2013). However, they contain varying assumptions about the lithospheric structure and composition, including the application of uniform values of radiogenic heat production for the upper and lower crust, or an exponential relationship of heat production with depth. These assumptions are not representative of the heat production sampled from numerous lithologies that constitute upper crustal rocks, neither in Antarctica (Burton-Johnson et al., 2017; Carson et al., 2014) nor globally (Gard et al., 2019; Hasterok et al., 2018). Heat producing elements (HPEs) are responsible for heat produced within the crust and preferentially concentrate into felsic rocks, but their distribution within these felsic rocks varies both spatially and temporally (Jaupart & Mareschal, 2003; McLaren et al., 2003; Perry et al., 2006).

Plate tectonic reconstructions (Figure 1) indicate that beneath the thick cover of ice, East Antarctica contains rocks with affiliations to Australia, Africa, and India (Aitken, Betts et al., 2016; Daczko et al., 2018; Ferraccioli et al., 2011; Flowerdew et al., 2013; Mulder et al., 2019), all of which were adjoined prior to the breakup of Gondwana during the Jurassic (Boger, 2011). Geochemical and geophysical studies indicate that both the observed heat flow and crustal heat production across these continents is highly variable (Carson et al., 2014; Cull, 1982; Hasterok & Gard, 2016; Jones, 1987; Nyblade et al., 1990; Roy & Rao, 2000). Heat flow in tectonically stable regions is largely controlled by crustal characteristics and the resulting crustal component of heat flow (Förster & Förster, 2000; Mareschal & Jaupart, 2013). As such, if southern Australia represents the true geological counterpart of East Antarctica, then we expect to observe similarly variable heat flow across their shared tectonic margin.

This study presents nine new heat flow measurements obtained from the Coompana Province, southern Australia (Figure 1), which fills a significant gap in the current Australian heat flow data set. These data are used to assess the magnitude and spatial variability of heat flow predicted for the corresponding domain of East Antarctica based on geophysical methods. Importantly, this includes the Totten Glacier catchment (purple dashed line in Figure 1c (Wright et al., 2012)), shown to be thinning at accelerated rates in comparison to other glacial regions of Antarctica (Aitken, Roberts et al., 2016; Pritchard et al., 2012). Our data are then combined with a global heat flow data set to assist in contextualizing the heat flow regime over a continental scale. This approach enables an evaluation of the degree of fit and associated uncertainty between measured heat flow values from conjugate terranes and the current geophysically derived models that constrain heat flow in East Antarctica.

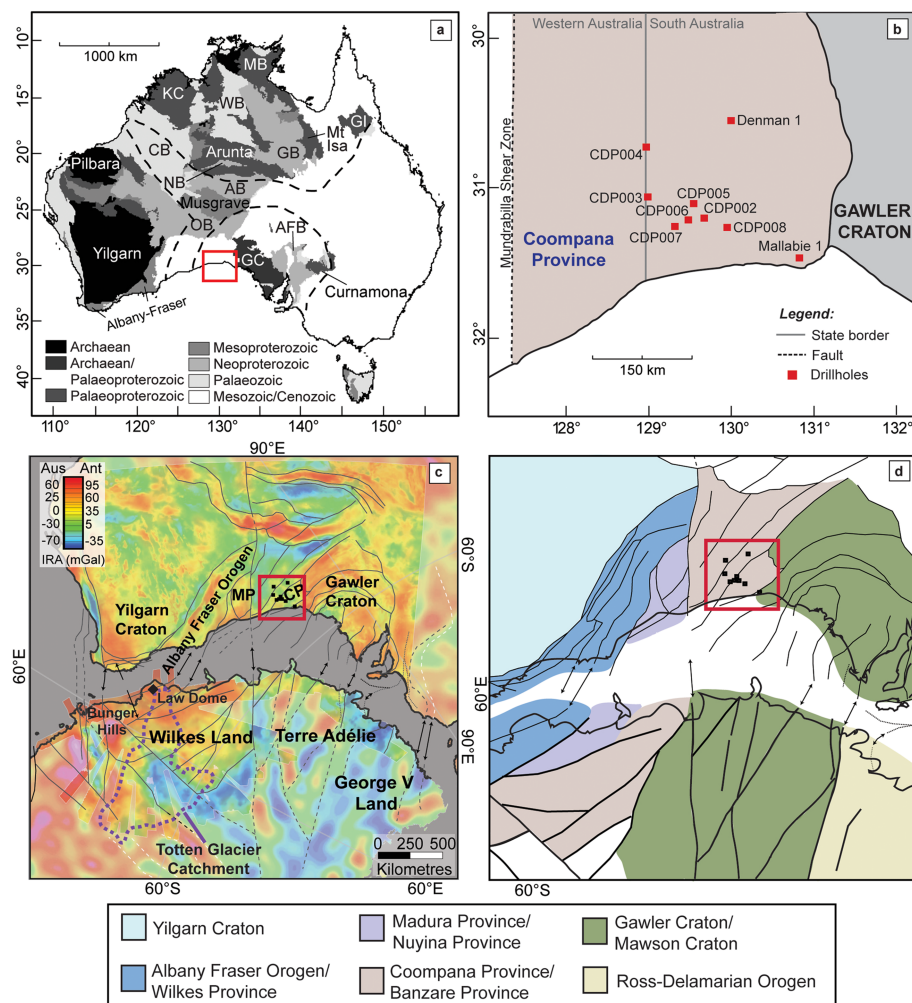


**Figure 1.** (a) Major tectonic provinces of Australia. Study location shown in Figure 1b outlined by red box. Abbreviations: AB, Amadeus Basin; AFB, Adelaide Fold Belt; CB, Canning Basin; GB, Georgina Basin; GC, Gawler craton; GI, Georgetown inlier; KC, Kimberley craton; MB, McArthur Basin; NB, Ngallia Basin; OB, Officer Basin; WB, Wiso Basin. Modified from Raimondo et al. (2014). (b) Locations of drill holes from the Coompana Province used in this study. (c) Total magnetic intensity anomalies overlain on a Leeuwin fit reconstruction at 160 Ma. Black symbols indicate drill hole locations used for heat flow measurements, and purple dashed line indicates the boundary of the Totten glacier catchment. Abbreviations: MP, Madura Province; CP: Coompana Province. Modified from Aitken et al. (2014). (d) Basement geology and tie points for the terrane correlation between southern Australia and East Antarctica. Modified from Aitken et al. (2014) and Maritati et al. (2019).

## 2. Geological Background

### 2.1. Tectonic Connections Between Southern Australia and Antarctica

The tectonic connections between Antarctica and its conjugate terranes play an important role in understanding the subglacial bedrock of Antarctica. At the formation of the supercontinent Gondwana, Antarctica was bound on all sides by Africa, South America, India, Australia, and Zealandia (Meert & Van Der Voo, 1997). Rifting between Australian and Antarctica commenced at approximately 160 Ma (Norvick & Smith, 2001; Totterdell et al., 2000), with Australia drifting northward while relatively, Antarctica remained stationary. A number of full-fit continental reconstructions currently exist that establish the relationship between the conjugate margins of southern Australia and East Antarctica (see Williams et al. (2019) for a review); these vary in their E-W alignment by up to ~380 km (see Figure 2 in Williams et al. (2019)). While several of these reconstructions remain viable, the “Leeuwin” fit is an

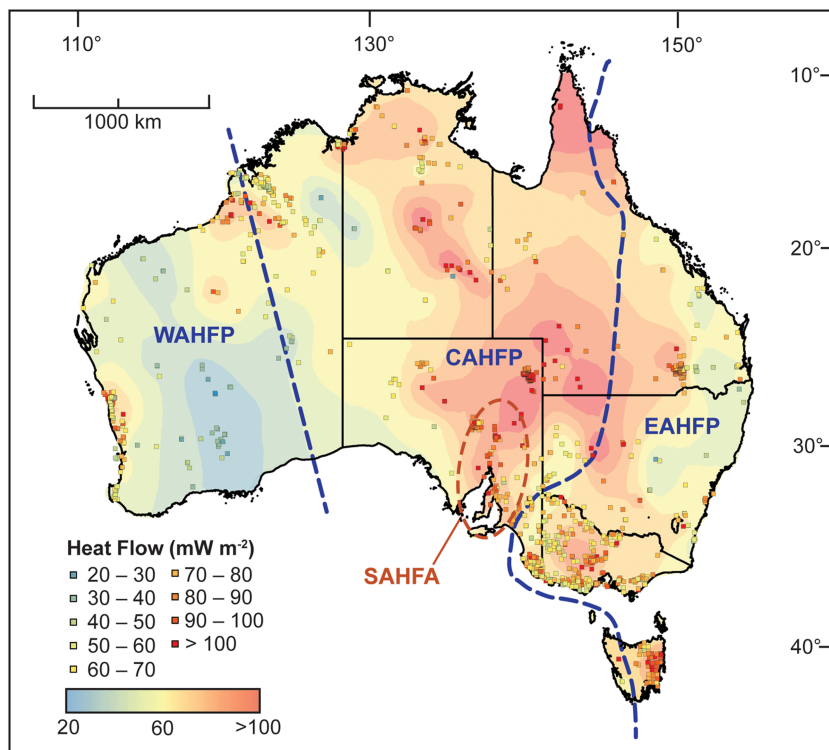


**Figure 2.** Current Australian heat flow data set. The Australian heat flow regime is defined by three major heat flow provinces: The western, central, and eastern heat flow provinces (abbreviated as WAHFP, CAHFP, and EAHFP, respectively). The south Australian heat flow anomaly (abbreviated as SAHFA) represents a region of anomalously elevated heat flow that dominates the southeastern portion of the CAHFP. The associated kriging uncertainty map is provided in figure S1 in the supporting information. References of constituent heat flow measurements are provided in table S1.

appropriate quantitative full-fit reconstruction that can reconcile a range of diverse geological and geophysical constraints (Williams et al., 2011). It is thus the preferred model used here and illustrated in Figure 1.

All available continental reconstructions indicate strong affiliations between the major tectonic provinces of southern Australia and East Antarctica (Aitken, Betts, et al., 2016; White et al., 2013). Starting in the west, the Yilgarn Craton (Figure 1a) is a granite-greenstone Archean crustal block (Champion & Cassidy, 2007) that occupies the majority of the Western Australian Craton and comprises some of the oldest known rocks on Earth (Wyche et al., 2019). It is not easily traced into East Antarctica, although reworked equivalents are found in the Bunger Hills region of far western Wilkes Land (Figure 1c; Daczko et al., 2018; Tucker et al., 2017). Further east, the Gawler Craton (Figure 1) contains crystalline basement that has experienced a complex tectonic history from the Archean to Mesoproterozoic (Daly et al., 1998; Hand et al., 2007), but has remained tectonically quiescent for the past billion years. It has a long-lived connection to the Archean-Paleoproterozoic rocks of the Mawson Craton of Terre Adélie in East Antarctica (Payne et al., 2009; Williams et al., 2017).

In Australia, these two ancient cratons are linked by the Mesoproterozoic Albany Fraser Orogen, Madura Province and Coompana Province. The Albany Fraser Orogen is NE-SW trending tectonic wedge that formed as a result of the two-stage assembly of Mesoproterozoic Australia (Clark et al., 2000). The Madura Province lies to the east of the Albany Fraser Orogen and is characterized by similar Mesoproterozoic lithologies to those of the adjacent Coompana Province, interpreted to have formed in an oceanic arc setting (Spaggiari et al., 2018). The two provinces are separated by the crustal-scale Mundrabilla Shear Zone (Figure 1b). The Coompana Province underlies thick Neoproterozoic to Tertiary sediment cover and is characterized by Mesoproterozoic gneissic and granitic rocks typical of the Musgrave orogenic system (Wade et al., 2008; Figure 1). Based on previous mineral exploration drilling

programs, it comprises four main supersuites (Jagodzinski et al., 2018; Wise et al., 2018): the Toolgana Supersuite (approximately 1,610 Ma) is interpreted to be derived from a subduction-enriched mantle source (Smithies et al., 2015a, 2015b); the Undawigi Supersuite (approximately 1,490 Ma) is interpreted as possible recycling of the arc crust of the Toolgana Supersuite (Kirkland et al., 2017a; Payne et al., 2007); the Moodini Supersuite (1,190–1,140 Ma) comprises plutons ranging from mafic to granitic in composition, intruded into the eastern Coompana Province (Hartnady et al., 2018); and lastly, the Warakurna Supersuite (approximately 1,080 Ma) represents a mafic intrusion (11 km in diameter) that forms part of the Coompana Magnetic anomaly (Foss et al., 2017; Wise et al., 2018).

In East Antarctica these Mesoproterozoic domains are broadly analogous to those of the Wilkes, Nuyina, and Banzare Provinces comprising much of Wilkes Land (Figure 1d; Aitken et al., 2014; Boger, 2011; Fitzsimons, 2003; Maritati et al., 2019). Recent zircon U-Pb-Hf geochronology undertaken on samples of crystalline basement from the Nuyina and Banzare Provinces reveal approximately 1,150 Ma plutons, with affinity to the Moodini Supersuite found within both the Madura and Coompana Provinces of southern Australia (Figures 1c and 1d). Furthermore, older xenocrystic zircon U-Pb-Hf signatures correlate with known magmatic suites within the Madura and Coompana Provinces, underscoring the relationship between the Madura/Nuyina and Coompana/Banzare Provinces (Figure 1d; Maritati et al., 2019). West of Law Dome, glacial sandstone erratic samples sourced from interior Wilkes Land are Neoproterozoic in age, with detrital zircon U-Pb-Hf signatures similar to the Australian Officer Basin (Figure 1a), suggesting the presence of an extensive region of sedimentary cover across interior Wilkes Land covering Mesoproterozoic basement (Maritati et al., 2019).

The correlation of aerogeophysical signatures, comparable age spectra, and isotopic characteristics from multiple locations along the conjugate margins of East Antarctica and southern Australia provides compelling evidence for similar crustal characteristics built and consolidated through a shared history during the Nuna-Rodinia-Gondwana supercontinent cycles. These once contiguous domains have remained tectonically quiescent (with the exception of the rifting that initiated their separation), indicating that the rocks exposed across southern Australia are representative of those that characterize the bedrock beneath the ice in previously contiguous regions of East Antarctica.

## 2.2. Heat Flow Map of Southern Australia

The oldest and coldest regions of southern Australia exist in the west, comprised mainly of the Archean Yilgarn Craton, which exhibits an average heat flow of  $39 \pm 8 \text{ mW/m}^2$  (Sass & Lachenbruch, 1979; Weber et al., 2011). This contrasts against the Central Australian Heat Flow Province (CAHFP; Figure 2), which comprises abnormally enriched Proterozoic crust with an average heat flow value of  $83 \pm 13 \text{ mW/m}^2$  (Cull, 1982; McLaren et al., 2003). Heat flow increases to  $>120 \text{ mW/m}^2$  throughout the South Australian Heat Flow Anomaly (SAHFA; Figure 2), a north-south trending region of anomalously elevated heat flow that extends north of the Adelaide Fold Belt (Neumann et al., 2000) on the eastern edge of the Gawler Craton (Figure 1a). Abnormal enrichment of HPEs (averaging  $6 \mu\text{W/m}^3$  and measured up to  $16 \mu\text{W/m}^3$  in the northern Adelaide Fold Belt) are responsible for the elevated heat flow observed here (McLaren et al., 2002; Sandiford et al., 2002); for comparison, global averages of granitic heat production are  $2.5\text{--}3.0 \mu\text{W/m}^3$  (Haenel et al., 1988; Vilà et al., 2010). Lastly, eastern Australia comprises the youngest portion of Australian crust which has been subjected to tectonic activity up until the Cenozoic, exhibiting heat flow values of  $72 \pm 27 \text{ mW/m}^2$  (Kirkby & Gerner, 2013; Mather et al., 2018; Matthews & Beardmore, 2007; Sass & Lachenbruch, 1979; Figure 2).

No *in situ* heat flow estimates exist from the Coompana Province; predictions of  $45\text{--}60 \text{ mW/m}^2$  for this region are interpolated from *in situ* measurements 540 km to the east and up to 900 km to the west (Beardmore & Hill, 2010; Raimondo et al., 2014). These approximations appear geologically reasonable, given that the Coompana Province comprises juvenile crust with oceanic affiliations (Kirkland et al., 2017b). Due to the mafic-intermediate nature of the basement lithologies, elevated heat flow is not expected (Beardmore & Cull, 2001). However, new surface heat flow estimates obtained as part of this study will test this hypothesis and fill a significant gap within the Australian continental data set, providing insights into the true thermal regime of the Coompana Province and the lithologies that contribute to its crustal heat production.

### 2.3. Heat Flow and Heat Production of East Antarctica

The conventional measurement of heat flow requires access to drill holes that have recovered core samples of bedrock and direct measurement of the thermal gradient downhole (Beardmore & Cull, 2001). While a small number of drill holes exist in Antarctica, they are extremely sparse in their distribution (Martos et al., 2017) and all measure thermal parameters only within ice or subglacial sediment; none yet have intersected the bedrock beneath (Goodge, 2018). Some measurements exist from offshore localities that sample sediment derived from the continental margin (Decker & Bucher, 1982; Dziadek et al., 2017; Morin et al., 2010). These measurements are not representative of onshore continental bedrock, as they are affected by advective flow at the surface and influenced by varied levels of sedimentation compared to heat flow onshore.

Minimal exposed rock outcrop exists along the coastal regions of East Antarctica from which to obtain in situ heat flow measurements. However, a recent study by Carson et al. (2014) provided heat production data along a 300-km transect in the Prydz Bay region, approximately 1,000 km west of Wilkes Land, with median heat production values ranging from 0.4 to 12.9  $\mu\text{W}/\text{m}^3$ . These values were assigned to a simple crustal model and an assumed mantle heat flow, from which average heat flow estimates of 31–83  $\text{mW}/\text{m}^2$  were derived. One additional heat flow estimate from the coastline of East Antarctica has been obtained from a temperature profile within the ice sheet at Law Dome (Figure 1c), which returned a heat flow estimate of 75  $\text{mW}/\text{m}^2$  (Dahl-Jensen et al., 1999). A limited number of heat flow measurements exist from regions of Antarctica further afield, derived from modeling englacial temperature profiles and radar data, as well as measurements into subglacial sediments. These estimates range from ~40 to 100  $\text{mW}/\text{m}^2$  (see Table S1 in Martos et al. (2017)).

## 3. Results

Heat flow was calculated for nine locations across the Coompana Province following the method of Gerner et al. (2012). The calculation of heat flow requires the collection of temperature data (obtained via a combination of continuous and stop-and-go down-hole wireline logging (Harris & Chapman, 2007)) and thermal conductivity data (obtained via the use of a Thermal Optical Scanner Apparatus (Popov et al., 1999)). Heat production data for the Coompana Province were obtained via geochemical analyses of 195 core samples, to assess the crustal contributions to the overall Coompana Province heat flow regime. Detailed heat flow methods, accompanied by individual descriptions of temperature, thermal conductivity and heat production data collection are found within the Methods section of the supporting information.

### 3.1. Temperature Data

Continuous temperature logs were obtained for seven of the eight holes drilled as part of the 2017 PACE Coompana Drilling Program (Figure 3). The thermal gradients of all holes are relatively similar, with no elevated outliers. Each log was conducted through the sedimentary cover sequences and into at least 100 m of crystalline basement. All logs were measured from the surface to depths ranging between 360 and 680 m, depending on the maximum drilling depth reached.

Repeat temperature logs were obtained for holes CDP002 and CDP004 24 hr after the initial logs were run (Figures S2 and S3). These data provide information about the manner in which the thermal gradient returned to equilibrium after drilling. Both repeat logs indicate a negative shift in temperature after 24 hrs, indicating that temperatures were cooling after the cessation of drilling. However, it should be noted that the repeat logs were only run within the casing string to 340- and 440 m depth, respectively, and not to total depth. Hence, they may not be representative of the temperature transition occurring deeper within the drill holes. The observed shifts in temperature are consistent with trends observed in Förster et al. (2001), indicating that heat flow determinations derived from this suite of nonequilibrium temperature logs should be regarded as minimum estimates.

### 3.2. Heat Production

A total of 195 samples were collected for geochemical analysis from the 2017 Coompana Drilling Program. The computed heat production for all samples can be found in Table S2. Figure 3 and Table 1 show the range of heat production values determined from samples collected within each hole. Most holes exhibit large

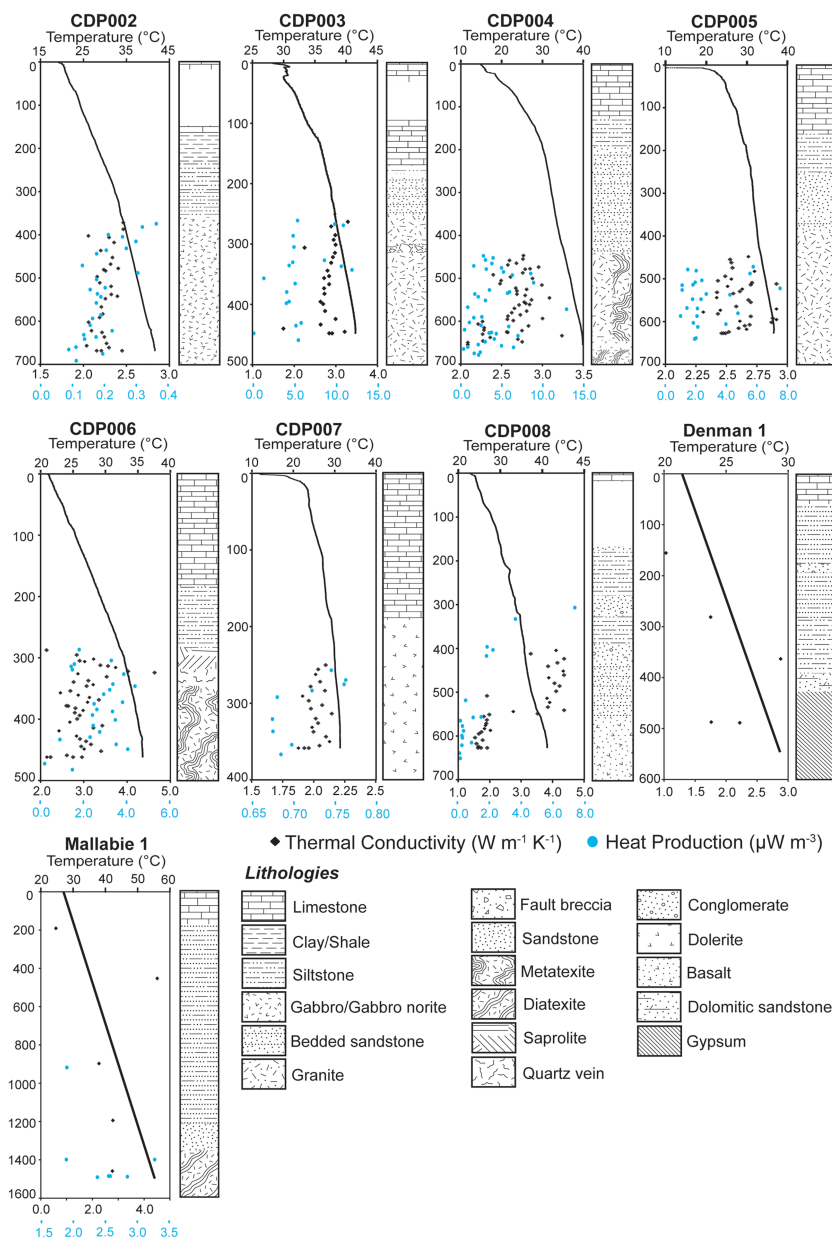


**Figure 3.** Temperature, thermal conductivity, heat production, and lithologies for the Coompana Province drill holes used to estimate surface heat flow.

ranges in heat production, with the greatest range recorded from CDP003 ( $0.25\text{--}12.06\text{ }\mu\text{W/m}^3$ ; Table 1); this hole also exhibited the highest mean value of  $5.46\text{ }\mu\text{W/m}^3$ . Two holes had noticeably low outputs of heat production that ranged from  $0.09$  to  $0.40\text{ }\mu\text{W/m}^3$  (CDP002) and  $0.71\text{--}0.81\text{ }\mu\text{W/m}^3$  (CDP007). The highest value of heat production ( $12.81\text{ }\mu\text{W/m}^3$ ) was recovered from an altered member of the Moodini Supersuite, enriched in uranium relative to other samples from this lithology. However, it is not representative of the average heat production analyzed for this drill hole or for any other samples analyzed as part of this study.

### 3.3. Thermal Conductivity and Heat Flow

A total of 281 samples across the eight Coompana Drilling Program holes were selected and measured for thermal conductivity. Table 2 shows a summary of the variations in thermal conductivity across each of the lithologies present. Conductivity ranged from  $0.85\text{ Wm/K}$  in a claystone sample, through to  $5.22\text{ Wm/K}$  from an aggregate of quartz clasts within a gravel conglomerate sample (Table 2); both end-members

**Table 1**

Summary of Drill Hole Characteristics, Calculated Heat Flow Values, Bottom Hole Temperatures, Heat Production Mean and Ranges, and Total Drilling Time (Spud Date Through to Date Total Depth Reached)

Drill hole name	Coordinates (WGS84)	Heat flow (mW/m <sup>2</sup> )	Bottom hole temperature recorded in drill hole	Heat production mean and range (μW/m <sup>3</sup> )	Total drilling time
CDP001	31°52'59"S, 129°25'48"E	N/A	N/A	4.49 (2.56–11.08)	41 days
CDP002	31°17'02"S, 129°40'32"E	55 ± 3	41 °C at 662 m	0.19 (0.08–0.36)	37 days
CDP003	31°09'06"S, 129°01'31"E	52 ± 4	36 °C at 446 m	5.46 (0.25–12.06)	33 days
CDP004	30°49'48"S, 129°00'45"E	62 ± 2	40 °C at 646 m	3.75 (0.38–12.81)	30 days
CDP005	31°11'37"S, 129°33'06"E	51 ± 2	36 °C at 635 m	2.67 (0.96–7.56)	24 days
CDP006	31°18'00"S, 129°29'27"E	68 ± 2	35 °C at 460 m	2.62 (0.20–4.41)	17 days
CDP007	31°20'36"S, 129°20'38"E	40 ± 2	31 °C at 358 m	0.71 (0.68–0.76)	7 days
CDP008	31°20'56"S, 129°56'21"E	70 ± 2	41 °C at 624 m	1.33 (0.09–7.38)	11 days
Mallabie 1	31°32'14"S, 130°36'06"E	52 ± 2	52 °C at 1493 m	1.39 (0.71–1.73)	45 days
Denman 1	30°39'20"S, 129°58'47"E	65 ± 3	30 °C at 232 m	N/A	27 days

represent reasonable values for their corresponding lithology (Beardmore & Cull, 2001). Figure 3 and Table 2 show the extent of thermal conductivities across the eight holes, with CDP008 accounting for not only the maximum and minimum thermal conductivities but also the largest spread between the first and third quartiles of the sample set. Similarly, CDP007 exhibits not only the smallest spread of thermal conductivities between samples but also the lowest values on average, corresponding to the lowest measured heat flow.

Figure 4 and Table 1 show the heat flow results calculated for the Coompana Province. Heat flow ranges from 40 to 70 mW/m<sup>2</sup>, with the lowest value of 40 mW/m<sup>2</sup> calculated from CDP007 and the highest value of 70 mW/m<sup>2</sup> calculated from CDP008. The mean heat flow for the region is 57 ± 3 mW/m<sup>2</sup>.

## 4. Discussion

### 4.1. Improvements to the Heat Flow Map of Southern Australia

Our study contributes new heat flow data to a largely unconstrained portion of southern Australia; it ensures a better understanding of the spatial variability of heat flow from the western Gawler Craton through to the Albany Fraser Orogen and Yilgarn Craton (Figure 1). Previously published heat flow maps (Beardmore & Hill, 2010; Raimondo et al., 2014) suggest that within the Gawler Craton, heat flow decreases from the east to west, with an average value of approximately 45–60 mW/m<sup>2</sup> for the central to western Gawler Craton (Cull, 1982; Figure 2). Throughout the Albany Fraser Orogen, the same heat flow maps estimate equivalent values of 45–60 mW/m<sup>2</sup>. However, these estimates are derived by interpolation of extremely sparse neighboring data, as no direct measurements exist in this region. Finally, the Yilgarn Craton is characterized by some

**Table 2**

Summary of Thermal Conductivity Values From Each of the Sampled Lithologies Across All Drill Holes in This Study

Lithology	Range of thermal conductivity (Wm/K)	Mean thermal conductivity (Wm/K)	Number of measurements
Basalt	1.53–3.52	1.89	17
Breccia	2.46–3.00	2.57	3
Conglomerate	3.30–5.22	4.21	3
Diatexite	2.07–3.24	2.63	41
Diorite	2.27–2.36	2.31	2
Dolerite	1.74–2.14	2.00	22
Gabbro/gabbro norite	1.99–2.34	2.17	30
Gneiss	2.86–4.02	3.28	8
Granite	2.43–3.29	2.80	68
Metasomatic rock	2.15–4.64	3.22	9
Metatexite	2.15–3.40	2.87	28
Sandstone	1.92–4.41	3.89	16
Saprolite	2.14–2.84	2.49	2
Siltstone	1.05–1.78	1.37	5

of the lowest heat flow values observed in Australia, averaging between 23 and 45 mW/m<sup>2</sup> (Howard & Sass, 1964; Munroe et al., 1975; Weber et al., 2011).

With the addition of the new Coompana Province heat flow data, we are able to confirm that previous predictions of heat flow for this region, based on kriging between nearest neighbors, are broadly reasonable. Our new estimates range from 40 to 70 mW/m<sup>2</sup> with an average of  $57 \pm 3$  mW/m<sup>2</sup>, consistent with the existing interpolated values of 45–60 mW/m<sup>2</sup> as stated above (Beardmore & Hill, 2010; Raimondo et al., 2014). Notably, the highest heat flow (CDP008;  $70 \pm 2$  mW/m<sup>2</sup>) corresponds to basaltic basement underlying ~550 m of sedimentary rocks. This may indicate that the sediments are providing a thermal blanketing effect to the heat flowing from below (Zhang, 1993). However, this conflicts with results from Mallabie 1, where more than 1,200 m of sedimentary units overly a diatexite basement and yet a low heat flow value of  $52 \pm 2$  mW/m<sup>2</sup> is obtained. In contrast, a sediment thickness of only 350 m for CDP006 produces an essentially identical value to CDP008 ( $68 \pm 2$  mW/m<sup>2</sup>). The elevation in heat flow observed for CDP006 and CDP008 may therefore indicate a more spatially extensive and higher heat produ-

cing unit at depth, which better signifies the character of the basement than the effects of thermal insulation from overlying sedimentary units.

Nevertheless, if sedimentary blanketing influences in some way the heat flow patterns across southern Australia, this process is likely also applicable to East Antarctica. U-Pb dating of detrital zircon and in situ authigenic monazite from the Wilkes Land Sabrina Sedimentary Basin returns Neoproterozoic ages that are comparable to Neoproterozoic sequences within the eastern Officer Basin (Figure 1a). This supports the existence of extensive sedimentary cover ( $100,000 \text{ km}^2$ ) across the Vanderford Glacier Catchment (located west of the Totten Glacier Catchment; Figure 1c), which may extend further east across Wilkes Land (Maritati et al., 2019).

Our new heat flow estimates provide in situ characterization of the Coompana Province heat flow regime and populate a significant gap within the Australian heat flow data set. With aerogeophysical and geochronological data confirming crustal-scale similarities between central southern Australia and the conjugate margin of East Antarctica, we are now able to apply the heat flow characterization of the Coompana Province as an estimation of the thermal regime in the formerly contiguous crust of Wilkes Land. Subsequently, we can use this to verify the heat flow characterization of East Antarctica derived from geophysical models.

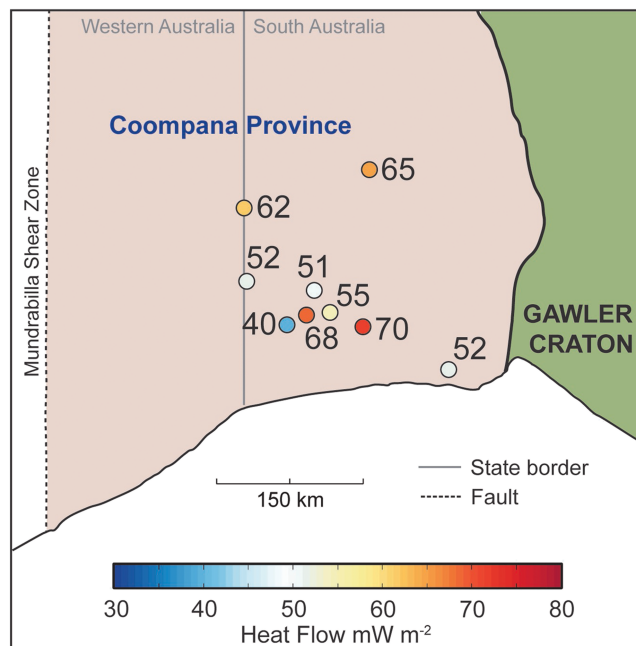


**Figure 4.** Heat flow estimates obtained from the Coompana Province drilling program (holes CDP002–CDP008). See Table 1 for data source.

#### 4.2. Existing Models of Antarctic Heat Flow

Due to the environmental, logistical, and financial challenges of drilling boreholes that intersect bedrock beneath thick ice cover, obtaining in situ terrestrial thermal data from Antarctica remains deeply problematic. Consequently, constraining heat flow across the Antarctic continent has been achieved by modeling, largely using data derived from continental-scale geophysical studies. These include satellite, airborne, and ground-sourced magnetic data (Fox Maule et al., 2005; Martos et al., 2017; Purucker, 2013) and seismic data (An et al., 2015; Shapiro & Ritzwoller, 2004). Additional studies have relied on the distribution of subglacial lakes across Antarctica (Siegent & Dowdeswell, 1996), or combined previous heat flow estimates with numerical modeling to determine continental heat flow (Pattyn, 2010; Pollard et al., 2005). The models of Shapiro and Ritzwoller (2004), Fox Maule et al. (2005), An et al. (2015), and Martos

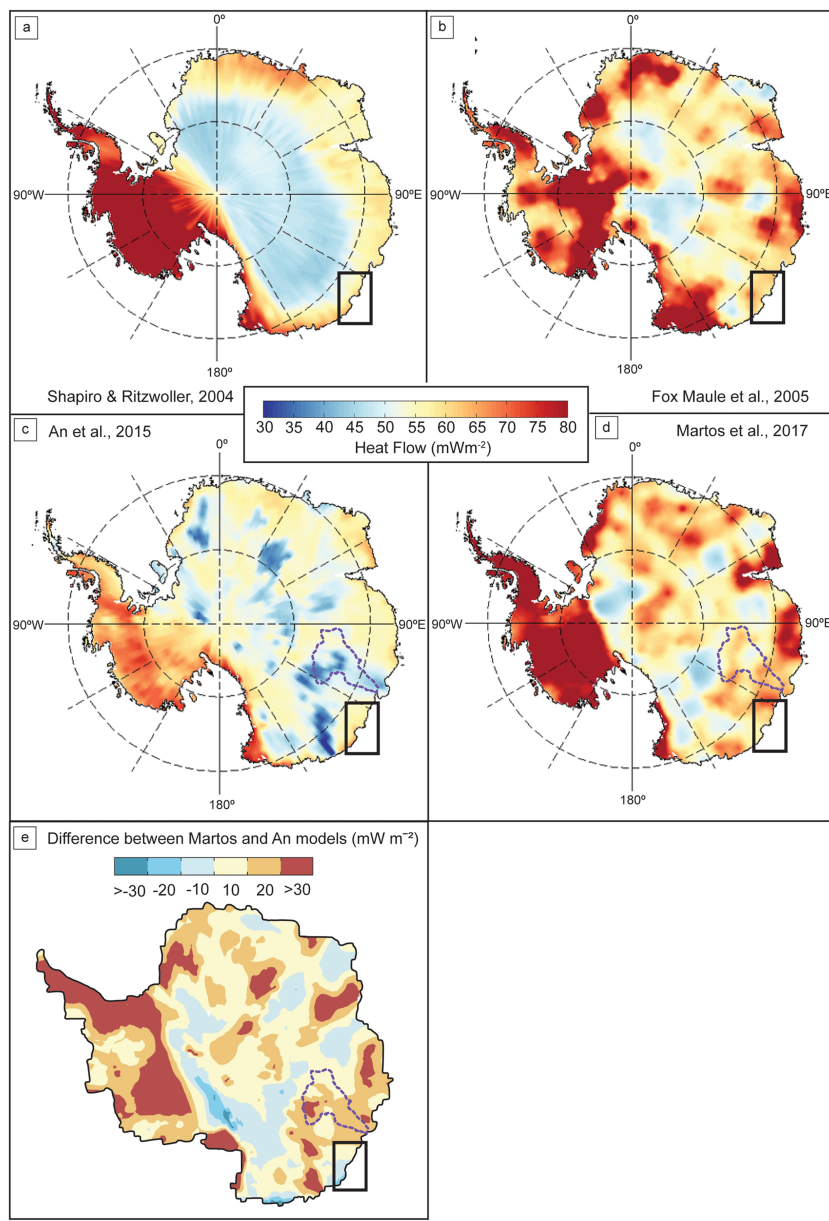


**Figure 5.** Four geophysically derived geothermal heat flux models for continental Antarctica, modified from Van Liefferinge et al. (2018). The models of (a) Shapiro and Ritzwoller (2004), (b) Fox Maule et al. (2005), (c) An et al. (2015), and (d) Martos et al. (2017) are plotted using the same color scale, truncated at 30 and 80 mW/m<sup>2</sup>; purple dashed line indicates the boundary of the Totten glacier catchment. (e) Observed difference between the Martos et al. (magnetic) and An et al. (seismic) models; purple dashed line indicates the boundary of the Totten glacier catchment. Black box represents the region of East Antarctica corresponding to the Coompana Province of southern Australia.

et al. (2017) will be the focus for comparison with our study (Figure 5), with particular emphasis on the two most recent models that employ the highest-resolution seismic and magnetic data.

While each successive heat flow model produced via geophysical approaches has been refined with improvements in the spatial resolution and accuracy of source data, significant disparities still exist between alternative models (Van Liefferinge & Pattyn, 2013). For the specific region of the East Antarctic coast once contiguous with the Coompana Province (outlined by the black box in Figure 5), differences of up to 25 mW/m<sup>2</sup> occur between the seismic models (An et al., 2015; Shapiro & Ritzwoller, 2004) and magnetic models (Fox Maule et al., 2005; Martos et al., 2017), while in adjacent regions of the East

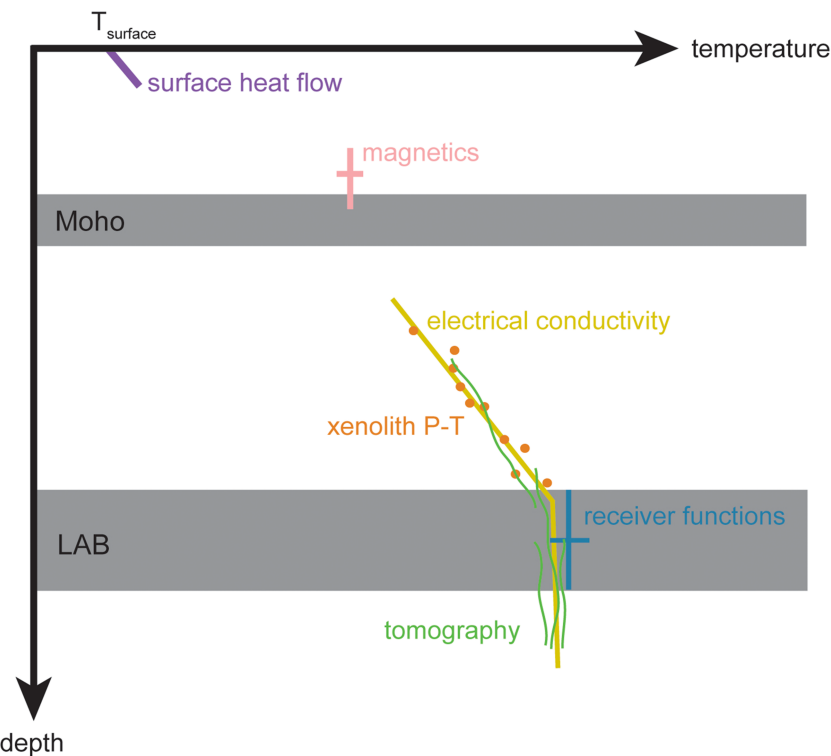


**Figure 6.** Comparison of geophysical and direct sampling techniques and their sensitivity to thermal properties with depth. With respect to this study, surface heat flow characterises the thermal regime of the upper crust, whereas magnetics are sensitive to the curie depth, deeper in the crust near the Moho boundary. Seismic methods are able to sense thermal properties within the upper mantle and discern temperatures at the lithosphere–asthenosphere boundary (LAB).

Antarctic coast, discrepancies exceed  $30 \text{ mW/m}^2$  (Figure 5e). Such disparities are nontrivial in the context of studies such as Llubes et al. (2006), which indicate that variations of  $20 \text{ mW/m}^2$  result in a change of up to  $15^\circ\text{C}$  for basal temperatures across East Antarctica. This is particularly important for the modeling of vulnerable regions such as the Totten Glacier catchment (Figure 1c), given that Figure 5e predicts discrepancies of  $10\text{--}30 \text{ mW/m}^2$  between magnetic and seismic heat flow models for this area.

Another consideration is the relatively large errors inherent to heat flow estimates from geophysical proxies. An et al. (2015) state that heat flow derived from their seismic model is only reliable to a maximum of  $90 \text{ mW/m}^2$ ; higher values of heat flow indicate either a weak lithospheric mantle or the presence of crustal melting (Jaupart & Mareschal, 2015). The Martos et al. (2017) magnetic model quotes errors of approximately  $10 \text{ mW/m}^2$  after applying the propagation equation for independent uncertainties.

In addition to their lack of agreement and inherent uncertainties, a large proportion of the thermal sensing derived from magnetic and seismic data is representative of lower crustal and upper mantle temperatures (Figure 6). Whereas magnetic methods sense temperatures in the lower crust and the upper mantle, corresponding to the deepest magnetic sources (assumed to be generally consistent with the Curie Depth isotherm, except where the deepest sources reach the Moho), seismic methods sense temperatures to much greater depths within the upper mantle, down to the lithosphere–asthenosphere boundary (LAB). Little information is thus gained about the upper crustal temperature regime, which limits the understanding of radiogenic heat produced from crustal sources and how it contributes to the overall heat flow.

Furthermore, geophysical models use simple layered crustal models (one- to two-layered crust) that field studies of heat production heterogeneity have repeatedly shown are not geologically realistic (Burton-Johnson et al., 2017; Carson et al., 2014; Hasterok et al., 2018; Sandiford et al., 2002). The models apply either constant thermal conductivity through a single crustal layer and assume laterally uniform crustal heat production (An et al., 2015), or an exponential relationship of decreasing heat production with depth (Martos et al.,

2017). In all cases, no lateral variation in crustal heat production within the Antarctic continent is accommodated. While changes in crustal heat flow (if great enough in magnitude) could be responsible for shallowing of the Curie depth as associated with the deepest magnetic sources, the outputs of these models do not allow the user to discern the source of the change.

#### 4.3. A Tectonically Reconstructed Heat Flow Map of Antarctica

As the availability of heat flow data is extremely limited across Antarctica, we propose using a tectonic reconstruction of the global heat flow data set to map the continent-wide heat flow distribution. This will assist in testing the validity of geophysically derived models by exploring the degree of fit between the modeled outputs of heat flow proximate to the East Antarctic coastline with measured *in situ* heat flow from the conjugate margins of Australia, India, and Africa.

The heat flow distributions relevant to the last supercontinent reconfiguration can be explored by plotting the currently available terrestrial heat flow data from each continent (Table S1; Hasterok, 2013) and anchoring each data point to its respective tectonic plate using GPlates software (Müller et al., 2018). A Leeuwin-hybrid reconstruction continental fit (Matthews et al., 2016) is then applied, and all data move relative to their original reference frame during plate rotation (Figure 7a). The data can then be interpolated to produce tectonically reconstructed heat flow maps (Figures 7b and 7c), enabling assessment of the degree of fit between the measured Gondwanan heat flow distribution and geophysically derived heat flow models of present-day Antarctica (Figures 7d and 7e).

Prior to the tectonic reconstruction being applied, sources of uncertainty in the Antarctic heat flow data set were evaluated and carefully filtered to exclude measurements that likely do not reflect conductive steady-state values. For example, Fisher et al. (2015) derive two significantly different heat flow values from subglacial Lake Whillans located on the West Antarctic Ice Sheet. Estimates from the sediments at the base of the lake result in a heat flow value of  $285 \text{ mW/m}^2$ , whereas heat flow derived from a temperature profile within the ice core to the base of the ice sheet indicates a value of  $110 \text{ mW/m}^2$ . This suggests that approximately  $175 \text{ mW/m}^2$  of heat has been lost in the process of melting the ice (Begeman et al., 2017; Fisher et al., 2015). Therefore, heat flow derived from ice cores that are positioned above localities of basal melting must be treated as minimum estimates. Heat flow values affected by advective systems still represent important information about the local thermal regime; however, when relating these values to models or measured estimates of conductive steady-state heat flow, a fair comparison cannot be made (Parrenin et al. 2017). Those measurements derived from temperature profiles taken only to shallow depths within the ice shelf are also treated with caution as significant extrapolation is required in order to obtain a temperature profile to the base of the ice sheet. Hence, measurements of heat flow from Antarctica with evidence for advective conditions, underlying meltwater and those derived from shallow temperature profiles were removed in the process of producing the heat flow maps in Figure 7.

To examine the heat flow distributions across the reconstructed terrane boundaries, a range of interpolation methods were tested in order to produce spatially continuous maps. Ordinary kriging, kernel smoothing, and local polynomial interpolation were critically assessed as outlined in the supporting information and Figures S8–S15. All three methods produced similar outputs between points of measurement (Figures 7b, S8, and S10), such that the map-scale heat flow patterns are largely insensitive to the chosen interpolation strategy. However, ordinary kriging produced the smallest associated prediction errors and is therefore the preferred method used to explore the global heat flow data set and its comparison to current models of Antarctic heat flow.

Our novel approach to comparing heat flow data across conjugate terranes requires consideration of the potential for tectonic alteration of the crust subsequent to rifting. We validated our method by plotting the global heat flow data set in GPlates and creating a tectonic plate reconstruction at 200 Ma (to ensure the close fit of Gondwanan conjugate margins prior to rifting). As shown in Figure S4, we successfully identify additional locations where heat flow trends are continuous across plate margins. A particularly strong correlation is observed across the northeastern South American Plate and the northwestern African Plate (Figure S5); a belt of low heat flow (generally lower than  $50 \text{ mW/m}^2$ ) is observed to extend ~4,000 km across this margin (Brigaud et al., 1985; Hamza & Muñoz, 1996). Elevated heat flow observed across the northern North West African Craton (Figure S6) corresponds to similar values on the conjugate coast of the

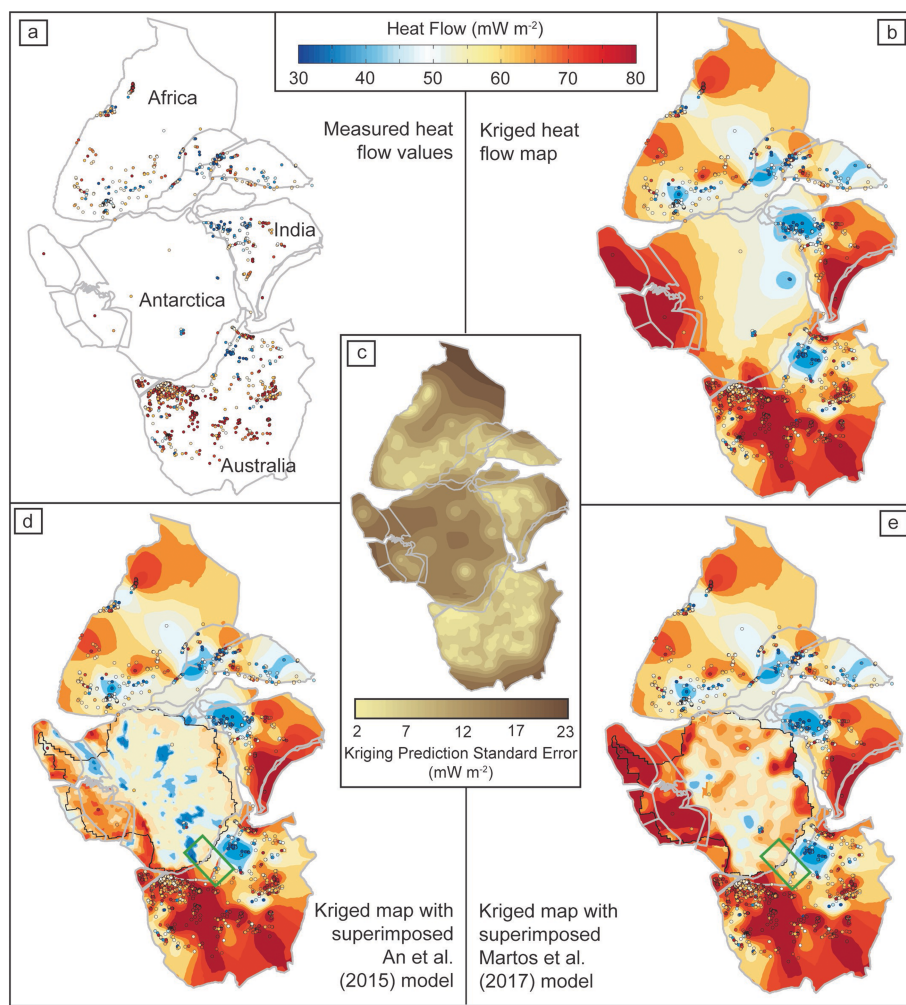


**Figure 7.** (a) Terrestrial heat flow data plotted on Gondwana reconstruction at 160 ma created using GPlates (Müller et al., 2018). No continental shelf heat flow data are included within this synthesis to ensure that all data values are representative of the stable onshore terrestrial thermal regime. (b) Kriged heat flow map. (c) Kriging prediction error map indicating the uncertainty associated with in situ data coverage relevant to Figures 7b, 7d, and 7e. (d) Heat flow model of An et al. (2015) superimposed in Figure 7b, with current Antarctic continental margin shown for reference (black line). Green rectangle indicates the conjugate alignment between the Coompana Province and Wilkes Land. (e) Heat flow model of Martos et al. (2017) superimposed in Figure 7b. Note that the modern coastline shown in Figures 7d and 7e is for illustrative purposes only and is not shown in a reconstructed position for the various tectonic elements of West Antarctica. Color scale is the same as used for Figure 2 and is truncated at 30 and 80  $\text{mW}/\text{m}^2$ .

northeastern North American Craton and Avalonian Plate, representing northeastern North America and southeastern Canada (Hyndman et al., 1979; Jaupart et al., 1982; Jessop & Judge, 1971; Rankin & Hyndman, 1971; Rimi, 1990). Further east, elevated heat flow observed in the North West African Plate also corresponds to similar values observed on the conjugate margin of the Iberian Plate (Figure S7), representing Andorra, Portugal, and Spain (Brigaud et al., 1985; Duque & Mendes-Victor, 1993; Fernández et al., 1998).

#### 4.4. Comparison With Geophysically Derived Heat Flow Models

The reconstructed Gondwanan heat flow map (Figure 7) leverages the similarity in crustal properties between each conjugate plate margin as a means to achieve two outcomes: (1) to predict the likely heat flow regime of the Antarctic continental margin by projecting the significantly greater data coverage of its formerly contiguous terranes into this region (Figure 7b) and (2) to compare this reconstructed distribution with both measured in situ heat flow values (Figure 7b) and estimates modeled from geophysical proxies (Figures 7d and 7e). As little is understood about the geology of the Antarctic interior and the uncertainty

of the reconstructed heat flow map is too large to be useful in this region (Figure 7c), the following discussion focuses on heat flow in regions proximal to the coastal perimeter of East Antarctica.

Coompana Province heat flow values ranging from 40 to 70 mW/m<sup>2</sup> correspond well to geophysically derived estimates of 50–70 mW/m<sup>2</sup> on the conjugate coast of Wilkes Land, East Antarctica. However, further east of the Coompana Province, elevated heat flow associated with the South Australian Heat Flow Anomaly that bounds the eastern Gawler Craton (SAHFA; Figure 2) is not reflected in geophysically derived models of the adjacent George V Coast (Figures 7d and 7e). This is despite the fact that the Delamerian Orogen of southern Australia and the Ross Orogen of East Antarctica represent conjugate arms of the same orogenic system (Flöttmann et al., 1993; Flöttmann & Oliver, 1994; Foden et al., 2006), and therefore should comprise an equivalent crustal composition associated with in situ heat flow measurements of up to 120 mW/m<sup>2</sup> (Neumann et al., 2000). Yet the An et al. (2015) model indicates an average heat flow of 55–60 mW/m<sup>2</sup> across George V Land, with a region of <40 mW/m<sup>2</sup> intersecting the coast directly adjacent to the projection of the SAHFA. The Martos et al. (2017) model indicates heat flow of ~60 mW/m<sup>2</sup> in this region, somewhat closer to the expected values based on our reconstruction but still substantially lower than is typical of the SAHFA.

Closer investigation of Figures 7d and 7e reveal areas of both good and poor correlation between the reconstructed heat flow map and geophysically derived models. The Martos model predicts substantially higher average heat flow across East Antarctica than the An model (and the Shapiro & Ritzwoller and Fox Maule models; Figure 5). This exacerbates a number of disparities juxtaposed against cooler regions of crust in both southern Western Australia (Yilgarn Craton and Albany Fraser Orogen) and southern India. Heat flow in southeastern Africa is highly variable; this pattern is similar to that observed in the An model. In contrast, there is no evidence from the An model that there are any regions of high Antarctic heat flow corresponding to the elevated values of northern India, yet the Martos model shows a circular feature of high heat flow at this location. Elevated heat flow at the southern edge of George V Land is imaged in all geophysical models and is a result of the West Antarctic Rift System, driven by recent magmatism and the likely presence of a magmatic plume (Ivins et al., 2017; Seroussi, Ivins et al., 2017).

#### 4.5. Implications for Accurately Mapping Antarctic Heat Flow

Geophysically derived heat flow models remain the best approach to understanding the Antarctic thermal regime at a continental scale. However, as outlined above, significant disparities remain between models derived from magnetic versus seismic data sets and their correlation to in situ measurements across reconstructed continental margins (Figure 7). Fundamentally, this highlights that in situ heat flow estimates represent different thermal states than those derived from geophysical models: the latter are well tuned to changes in mantle/lower crustal heat flow over continental scales, whereas the former integrate variations in upper crustal heat flow at local and regional scales (Figure 6).

Importantly, variations in heat flow observed at the surface (i.e., those most relevant to ice sheet stability) are a result of contributions from both mantle heat flow and/or radiogenic heat produced within the crust. This means that the crustal contribution to surface heat flow is critically important to constrain via in situ measurements, particularly given that in stable cratonic regions such as Antarctica and southern Australia, mantle heat flow variations are likely to be small (<10 mW/m<sup>2</sup>; Hasterok & Gard, 2016). As a result, it is unlikely that heat flow trends reflect fluctuations in mantle heat flow; rather, numerous studies from southern Australia confirm that the predominant cause is heterogeneous crustal heat production (McLaren et al., 2002; McLaren et al., 2003; Neumann et al., 2000; Sandiford et al., 2002). Provided that conjugate crustal blocks experience no tectonic reworking subsequent to rifting (i.e., the crust remains similar thickness on both sides, outside of the rift margins), their average heat production will remain comparable. It is therefore reasonable to expect that the observed variations in heat flow along the East Antarctic coast are largely attributed to variations in crustal heat production.

This conclusion has critical implications for the scale of observation relevant to improved ice sheet predictions: several ice flow studies indicate that variations in heat flow even on the local scale can result in melting (Fahnestock et al., 2001; Greve & Hutter, 1995; Winsborrow et al., 2010). These local variations, when attributed to shallow rather than deep-seated heat sources, indicate that geophysical models require further parameterization of the crustal component of heat flow in order to accurately inform ice sheet models. Furthermore, the simplified crustal architectures used within models are inherent limitations, because

they make invalid assumptions about the thermal uniformity of any given vertical crustal profile (thermal conductivity and crustal heat production). It is also difficult to determine where the thermal regime is conductive versus advective, which may be of critical importance to local conditions at the base of the ice sheet. The most significant improvement for future models of Antarctic heat flow derived from geophysical data is a more representative model of the three-dimensional crustal architecture and resultant variations of heat production within the crust (Goodge, 2018).

Any approach used to determine the spatial variability of heat flow across Antarctica will encounter limitations due to the inaccessibility of the bedrock that lies beneath the ice. This study shows that using heat flow values from conjugate terranes that are considerably more accessible is an effective, low cost, and practical approach, at least for direct correlatives along the Antarctic continental margin. Nevertheless, before this method can be extended to inland Antarctica with a high level of confidence, in-depth geostatistical analyses of the outputs of kriging interpolation are required, similar to that undertaken by Szwilus et al. (2019). This will permit more robust analysis of heat flow trends determined by kriging where heat flow data do not exist. Further improvement of the geological characterization of this region is also needed, given its comparative uncertainty, including in situ heat flow measurements wherever feasible as a critical validation parameter. Where significant variations between alternative models and in situ measurements currently exist, this discrepancy begs the question of whether its origin lies with poor data coverage or purely methodological differences (e.g., crustal versus mantle contribution to heat flow), and thus whether the modeled values remain acceptable. In particular, where crustal thickness, mantle heat flow, and the thermal regime (advective or conductive) are comparable and a similar neotectonic history is shared, variations in heat flow estimates may be indicative of differences in crustal heat production, and consequently, differences in crustal heat flow.

## 5. Conclusion

### Acknowledgments

Alan Aitken, Jörg Ebbing, and an anonymous reviewer are thanked for their comments which greatly improved the manuscript. Thorsten Becker is thanked for his editorial handling. Amy Lockheed, Luke Tylkowski, Tom Wise, Elizabeth Jagodzinski, and Sarlae McAlpine are thanked for their assistance in collecting temperature data throughout the PACE Coompana Drilling Program. Robert Aebi is thanked for his technical assistance in the field, and Stefan Peters for his assistance with the production of parts of Figure 7. Funding for this work was provided by the UniSA Research Themes Investment Scheme, and A. Pollett is supported by an Australian Government Research Training Program (RTP) Scholarship. J. Halpin is supported under the Australian Research Council's Special Research Initiative for Antarctic Gateway Partnership SR140300001. The Australian Research Council is acknowledged for support of this project via discovery projects DP180104074 and DP0987765. We also acknowledge Auscope for part funding of the downhole temperature logging equipment used in this study. Thermal conductivity and temperature data used to calculate heat flow values for the Coompana Province are available at the South Australian Geodata Database (<https://minerals.sarig.sa.gov.au/>). The global heat flow database can be accessed via <http://www.heatflow.org/>.

This study presents new heat flow estimates of 40–70 mW/m<sup>2</sup> from the Coompana Province, southern Australia, and provides the first thermal characterization of this significant gap in the Australian heat flow map. East Antarctica remains largely inaccessible for in situ heat flow measurements and therefore presents a significant challenge to better characterizing thermal conditions at the bedrock-ice interface. To provide an alternative approach to this problem, we offer a Gondwanan synthesis of all available in situ measurements from formerly contiguous terranes as a means to validate geophysically derived heat flow models. In this context, the new Coompana Province heat flow values compare favorably to the most recent geophysically derived estimates of 50–75 mW/m<sup>2</sup> for the Totten Glacier catchment of East Antarctica. However, our reconstructed map demonstrates that the heat flow distribution of southern Australia is highly variable and yet this heterogeneity is not reflected in corresponding geophysical models of East Antarctica, which are likely underestimating the contribution from crustal radiogenic heat production. Improved mapping of crustal heat production in East Antarctica and its influence on the resulting heat flow distribution will provide future studies the best opportunity for thermal characterization of East Antarctic crust and its role in current and predicted ice sheet movement.

## References

- Aitken, A. R. A., Betts, P. G., Young, D. A., Blankenship, D. D., Roberts, J. L., & Siegert, M. J. (2016). The Australo-Antarctic Columbia to Gondwana transition. *Gondwana Research*, 29, 136–152. <https://doi.org/10.1016/j.gr.2014.10.019>
- Aitken, A. R. A., Roberts, J. L., Ommen, T. D., Young, D. A., Golledge, N. R., Greenbaum, J. S., et al. (2016). Repeated large-scale retreat and advance of Totten glacier indicated by inland bed erosion. *Nature*, 533(7603), 385–389. <https://doi.org/10.1038/nature17447>
- Aitken, A. R. A., Young, D. A., Ferraccioli, F., Betts, P. G., Greenbaum, J. S., Richter, T. G., et al. (2014). The subglacial geology of Wilkes Land, East Antarctica. *Geophysical Research Letters*, 41, 2390–2400. <https://doi.org/10.1002/2014GL059405>
- An, M., Wiens, D. A., Zhao, Y., Feng, M., Nyblade, A., Kanao, M., et al. (2015). Temperature, lithosphere–asthenosphere boundary, and heat flux beneath the Antarctic plate inferred from seismic velocities. *Journal of Geophysical Research: Solid Earth*, 120, 8720–8742. <https://doi.org/10.1002/2015JB011917>
- Beardmore, G. R., & Cull, J. P. (2001). *Crustal Heat Flow: A Guide to Measurement and Modelling*. Melbourne: Cambridge University Press.
- Beardmore, G. R., & Hill, A. (2010). *Australia - Country Update*. Bali: Paper presented at the World Geothermal Congress.
- Begeman, C. B., Tulaczyk, S. M., & Fisher, A. T. (2017). Spatially variable geothermal heat flux in West Antarctica: Evidence and implications. *Geophysical Research Letters*, 44, 9823–9832. <https://doi.org/10.1002/2017GL075579>
- Boyer, S. D. (2011). Antarctica — Before and after Gondwana. *Gondwana Research*, 19, 335–371. <https://doi.org/10.1016/j.gr.2010.09.003>
- Brigaud, F., Lucazeau, F., Ly, S., & Sauvage, J. F. (1985). Heat flow from the west African shield. *Geophysical Research Letters*, 12, 549–552. <https://doi.org/10.1029/GL012i009p00549>

- Burton-Johnson, A., Halpin, J. A., Whittaker, J. M., Graham, F. S., & Watson, S. J. (2017). A new heat flux model for the Antarctic peninsula incorporating spatially variable upper crustal radiogenic heat production. *Geophysical Research Letters*, 44, 5436–5446. <https://doi.org/10.1002/2017GL073596>
- Carson, C. J., McLaren, S., Roberts, J. L., Boger, S. D., & Blankenship, D. D. (2014). Hot rocks in a cold place: High sub-glacial heat flow in East Antarctica. *Journal of the Geological Society*, 171, 9–12. <https://doi.org/10.1144/jgs2013-030>
- Champion, D., & Cassidy, K. (2007). An overview of the Yilgarn craton and its crustal evolution. *Geoscience Australia Record*, 14, 8–13.
- Clark, D. J., Hensen, B. J., & Kinny, P. D. (2000). Geochronological constraints for a two-stage history of the Albany–Fraser Orogen, Western Australia. *Precambrian Research*, 102, 155–183. [https://doi.org/10.1016/S0301-9268\(00\)00063-2](https://doi.org/10.1016/S0301-9268(00)00063-2)
- Cull, J. P. (1982). An appraisal of Australian heat-flow data. *BMR Journal of Australian Geology & Geophysics*, 7, 11–21.
- Daczko, N. R., Halpin, J. A., Fitzsimons, I. C. W., & Whittaker, J. M. (2018). A cryptic Gondwana-forming orogen located in Antarctica. *Scientific Reports*, 8, 8371. <https://doi.org/10.1038/s41598-018-26530-1>
- Dahl-Jensen, D., Morgan, V. I., & Elcheikh, A. (1999). Monte Carlo inverse modelling of the law dome (Antarctica) temperature profile. *Annals of Glaciology*, 29, 145–150. <https://doi.org/10.3189/172756499781821102>
- Daly, S. J., Fanning, C. M., & Fairclough, M. C. (1998). Tectonic evolution and exploration potential for the Gawler craton, South Australia. *AGSO Journal of Australian Geology and Geophysics*, 17, 145–168.
- Decker, E., & Bucher, G. (1982). Geothermal studies in the Ross Island-Dry Valley region. *Antarct Geoscience*, 4, 887–894.
- DeConto, R. M., & Pollard, D. (2016). Contribution of Antarctica to past and future sea-level rise. *Nature*, 531, 591. <https://doi.org/10.1038/nature17145>
- Duque, M. R., & Mendes-Victor, L. A. (1993). Heat flow and deep temperature in South Portugal. *Studia Geophysica et Geodaetica*, 37, 279–292. <https://doi.org/10.1007/bf01624601>
- Dziadek, R., Gohl, K., Diehl, A., & Kaul, N. (2017). Geothermal heat flux in the Amundsen Sea sector of West Antarctica: New insights from temperature measurements, depth to the bottom of the magnetic source estimation, and thermal modeling. *Geochemistry, Geophysics, Geosystems*, 18, 2657–2672. <https://doi.org/10.1002/2016GC006755>
- Fahnestock, M., Abdalati, W., Joughin, I., Brozena, J., & Gogineni, P. (2001). High geothermal heat flow, basal melt, and the origin of rapid ice flow in Central Greenland. *Science*, 294, 2338–2342. <https://doi.org/10.1126/science.1065370>
- Fernández, M., Marzán, I., Correia, A., & Ramalho, E. (1998). Heat flow, heat production, and lithospheric thermal regime in the Iberian Peninsula. *Tectonophysics*, 291, 29–53. [https://doi.org/10.1016/S0040-1951\(98\)00029-8](https://doi.org/10.1016/S0040-1951(98)00029-8)
- Ferraccioli, F., Finn, C. A., Jordan, T. A., Bell, R. E., Anderson, L. M., & Damaske, D. (2011). East Antarctic rifting triggers uplift of the Gamburtsev Mountains. *Nature*, 479, 388. <https://doi.org/10.1038/nature10566>
- Fisher, A. T., Mankoff, K. D., Tulaczyk, S. M., Tyler, S. W., & Foley, N. (2015). High geothermal heat flux measured below the West Antarctic ice sheet. *Science Advances*, 1. <https://doi.org/10.1126/sciadv.1500093>
- Fitzsimons, I. C. W. (2003). Proterozoic basement provinces of southern and southwestern Australia, and their correlation with Antarctica. *Geological Society, London, Special Publications*, 206, 93–130. <https://doi.org/10.1144/gsl.sp.2003.206.01.07>
- Flöttmann, T., Gibson, G. M., & Kleinschmidt, G. (1993). Structural continuity of the Ross and Delamerian orogens of Antarctica and Australia along the margin of the paleo-Pacific. *Geology*, 21, 319–322. [https://doi.org/10.1130/0091-7613\(1993\)021<0319:scotra>2.3.co;2](https://doi.org/10.1130/0091-7613(1993)021<0319:scotra>2.3.co;2)
- Flöttmann, T., & Oliver, R. (1994). Review of Precambrian-Palaeozoic relationships at the craton margins of southeastern Australia and adjacent Antarctica. *Precambrian Research*, 69, 293–306. [https://doi.org/10.1016/S0301-9268\(94\)90093-0](https://doi.org/10.1016/S0301-9268(94)90093-0)
- Flowerdew, M. J., Tyrrell, S., Boger, S. D., Fitzsimons, I. C. W., Harley, S. L., Mikhalsky, E. V., & Vaughan, A. P. M. (2013). Pb isotopic domains from the Indian Ocean sector of Antarctica: Implications for past Antarctica–India connections. *Geological Society, London, Special Publications*, 383. <https://doi.org/10.1144/sp383.3>
- Foden, J., Elburg, M. A., Dougherty-Page, J., & Burtt, A. (2006). The timing and duration of the Delamerian orogeny: Correlation with the Ross Orogen and implications for Gondwana assembly. *The Journal of Geology*, 114, 189–210. <https://doi.org/10.1086/499570>
- Förster, A., & Förster, H. J. (2000). Crustal composition and mantle heat flow: Implications from surface heat flow and radiogenic heat production in the Variscan Erzgebirge (Germany). *Journal of Geophysical Research*, 105(B12), 27,917–27,938. <https://doi.org/10.1029/2000JB900279>
- Förster, A., Merriam, F. D., & Davis, C. J. (2001). Spatial analysis of temperature (BHT/DST) data and consequences for heat-flow determination in sedimentary basins. *Geologische Rundschau*, 86, 252–261. <https://doi.org/10.1007/s005310050138>
- Foss, C., Reed, G., Keeping, T., Wise, T., & Dutch, R. (2017). Source magnetisation studies of the reverse magnetic anomalies in the Coompana area. Retrieved from Adelaide:
- Fox Maule, C., Purucker, M. E., Olsen, N., & Mosegaard, K. (2005). Heat flux anomalies in Antarctica revealed by satellite magnetic data. *Science*, 309(5733), 464–467. <https://doi.org/10.1126/science.1106888>
- Fretwell, P., Pritchard, H. D., Vaughan, D. G., Bamber, J., Barrand, N., Bell, R., & Casassa, G. (2013). Bedmap2: Improved ice bed, surface and thickness datasets for Antarctica. *The Cryosphere*, 7, 375–393. <https://doi.org/10.5194/tc-6-4305-2012>
- Gard, M., Hasterok, D., & Halpin, J. A. (2019). Global whole-rock geochemical database compilation. *Earth System Science Data*, 11(4), 1553–1566. <https://doi.org/10.5194/essd-11-1553-2019>
- Gerner, E. J., Kirkby, A. L., & Ayling, B. F. (2012). Heat Flow Determinations for the Australian Continent: Release 4. Retrieved from Goodge, J. W. (2018). Crustal heat production and estimate of terrestrial heat flow in central East Antarctica, with implications for thermal input to the East Antarctic ice sheet. *The Cryosphere*, 12.
- Greve, R., & Hutter, K. (1995). Polythermal three-dimensional modelling of the Greenland ice sheet with varied geothermal heat flux. *Annals of Glaciology*, 21, 8–12. <https://doi.org/10.3189/S0260305500015524>
- Haenel, R., Stegenga, L., & Rybach, L. (1988). *Handbook of terrestrial heat-flow density determination: with guidelines and recommendations of the International Heat Flow Commission* (Vol. 1): Springer Science & Business Media.
- Hamza, V. M., & Muñoz, M. (1996). Heat flow map of South America. *Geothermics*, 25, 599–646. [https://doi.org/10.1016/S0375-6505\(96\)00025-9](https://doi.org/10.1016/S0375-6505(96)00025-9)
- Hand, M., Reid, A., & Jagodzinski, L. (2007). Tectonic framework and evolution of the Gawler craton, southern Australia. *Economic Geology*, 102(8), 1377–1395. <https://doi.org/10.2113/gsecongeo.102.8.1377>
- Harris, R. N., & Chapman, D. S. (2007). Stop-go temperature logging for precision applications. *Geophysics*, 72, 119–123. <https://doi.org/10.1190/1.2734382>
- Hartnady, M. I. H., Kirkland, C. L., Dutch, R. A., Bodorkos, S., & Jagodzinski, E. (2018). Zircon HF isotopic signatures of the Coompana Province in South Australia. Retrieved from
- Hasterok, D. (2013). A heat flow based cooling model for tectonic plates. *Earth and Planetary Science Letters*, 361, 34–43. <https://doi.org/10.1016/j.epsl.2012.10.036>

- Hasterok, D., & Gard, M. (2016). Utilizing thermal isostasy to estimate sub-lithospheric heat flow and anomalous crustal radioactivity. *Earth and Planetary Science Letters*, 450, 197–207. <https://doi.org/10.1016/j.epsl.2016.06.037>
- Hasterok, D., Gard, M., & Webb, J. (2018). On the radiogenic heat production of metamorphic, igneous, and sedimentary rocks. *Geoscience Frontiers*, 9(6), 1777–1794. <https://doi.org/10.1016/j.gsf.2017.10.012>
- Howard, L. E., & Sass, J. H. (1964). Terrestrial heat flow in Australia. *Journal of Geophysical Research*, 69, 1617–1626. <https://doi.org/10.1029/JZ069i008p01617>
- Hyndman, R. D., Jessop, A. M., Judge, A. S., & Rankin, D. S. (1979). Heat flow in the maritime provinces of Canada. *Canadian Journal of Earth Sciences*, 16, 1154–1165. <https://doi.org/10.1139/e79-102>
- Ivins, E., Seroussi, H., Wiens, D., & Bondzio, J. (2017). West Antarctic Mantle Plume Hypothesis and Basal Water Generation. Paper presented at the EGU General Assembly Conference Abstracts.
- Jagodzinski, E., Bodorkos, S., & Crowley, J. L. (2018). *U-Pb Geochronology of the Eastern Coompana Province, South Australia*. South Australia: Retrieved from Adelaide.
- Jaupart, C., Mann, J. R., & Simmons, G. (1982). A detailed study of the distribution of heat flow and radioactivity in New Hampshire (U.S. A.). *Earth and Planetary Science Letters*, 59, 267–287. [https://doi.org/10.1016/0012-821X\(82\)90131-5](https://doi.org/10.1016/0012-821X(82)90131-5)
- Jaupart, C., & Mareschal, J. C. (2003). Constraints on crustal heat production from heat flow data. In H. D. Holland, & K. K. Turekian (Eds.), *Treatise on Geochemistry* (pp. 65–84). Oxford: Pergamon.
- Jaupart, C., & Mareschal, J. C. (2015). Heat flow and thermal structure of the lithosphere. In G. Schubert (Ed.), *Treatise on Geophysics (Second Edition)* (pp. 217–253). Oxford: Elsevier.
- Jessop, A. M., & Judge, A. S. (1971). Five measurements of heat flow in southern Canada. *Canadian Journal of Earth Sciences*, 8(6), 711–716. <https://doi.org/10.1139/e71-069>
- Jones, M. Q. W. (1987). Heat flow and heat production in the Namaqua Mobile Belt, South Africa. *Journal of Geophysical Research*, 92, 6273–6289. <https://doi.org/10.1029/JB092iB07p06273>
- Kirkby, A. L., & Gerner, E. J. (2013). Heat Flow Determinations for the Australian Continent: Release 5. Retrieved from
- Kirkland, C. L., Smithies, R. H., Spaggiari, C. V., Wingate, M. T. D., Quentin de Gromard, R., Clark, C., et al. (2017a). Proterozoic crustal evolution of the Eucla basement, Australia: Implications for destruction of oceanic crust during emergence of Nuna. *Lithos*, 278–281, 427–444. <https://doi.org/10.1016/j.lithos.2017.01.029>
- Kirkland, C. L., Smithies, R. H., Spaggiari, C. V., Wingate, M. T. D., Quentin de Gromard, R., Clark, C., et al. (2017b). Proterozoic crustal evolution of the Eucla basement, Australia: Implications for destruction of oceanic crust during emergence of Nuna. *Lithos*, 278, 427–444. <https://doi.org/10.1016/j.lithos.2017.01.029>
- Llubes, M., Lanseau, C., & Rémy, F. (2006). Relations between basal condition, subglacial hydrological networks and geothermal flux in Antarctica. *Earth and Planetary Science Letters*, 241, 655–662. <https://doi.org/10.1016/j.epsl.2005.10.040>
- Mareschal, J.-C., & Jaupart, C. (2013). Radiogenic heat production, thermal regime and evolution of continental crust. *Tectonophysics*, 609, 524–534. <https://doi.org/10.1016/j.tecto.2012.12.001>
- Maritati, A., Halpin, J. A., Whittaker, J. M., & Daczko, N. R. (2019). Fingerprinting Proterozoic bedrock in interior Wilkes Land, East Antarctica. *Scientific Reports*, 9, 10192. <https://doi.org/10.1038/s41598-019-46612-y>
- Martos, Y. M., Catalán, M., Jordan, T. A., Golynsky, A., Golynsky, D., Eagles, G., & Vaughan, D. G. (2017). Heat flux distribution of Antarctica unveiled. *Geophysical Research Letters*, 44, 11,417–411,426. <https://doi.org/10.1002/2017GL075609>
- Mather, B., McLaren, S., Taylor, D., Roy, S., & Moresi, L. (2018). Variations and controls on crustal thermal regimes in southeastern Australia. *Tectonophysics*, 723, 261–276. <https://doi.org/10.1016/j.tecto.2017.12.015>
- Matthews, C., & Beardsmore, G. (2007). New heat flow data from South-Eastern South Australia. *Exploration Geophysics*, 38, 260–269. doi: [doi:10.1071/EG07028](https://doi.org/10.1071/EG07028)
- Matthews, K., Maloney, K., Zahirovic, S., Williams, S., Seton, M., & Müller, D. (2016). Global plate boundary evolution and kinematics since the late Paleozoic. *Global and Planetary Change*, 146, 226–250. <https://doi.org/10.1016/j.gloplacha.2016.10.002>
- McLaren, S., Dunlap, W. J., Sandiford, M., & McDougall, I. (2002). Thermochronology of high heat-producing crust at mount painter, South Australia: Implications for tectonic reactivation of continental interiors. *Tectonics*, 21(4), TC001275. <https://doi.org/10.1029/2000tc001275>
- McLaren, S., Sandiford, M., Hand, M., Neumann, N., Wyborn, L., & Bastrakova, I. (2003). The hot southern continent: Heat flow and heat production in Australian Proterozoic terranes. *Special Papers - Geological Society of America*, 372, 157–167.
- Meert, J. G., & van Der Voo, R. (1997). The assembly of Gondwana 800–550 ma. *Journal of Geodynamics*, 23, 223–235. [https://doi.org/10.1016/S0264-3707\(96\)00046-4](https://doi.org/10.1016/S0264-3707(96)00046-4)
- Morin, R. H., Williams, T., Henrys, S. A., Magens, D., Niessen, F., & Hansaraj, D. (2010). Heat flow and hydrologic characteristics at the AND-1B borehole, ANDRILL McMurdo ice shelf project, Antarctica. *Geosphere*, 6, 370–378. <https://doi.org/10.1130/ges00512.1>
- Mulder, J. A., Halpin, J. A., Daczko, N. R., Orth, K., Meffre, S., Thompson, J. M., & Morrissey, L. J. (2019). A multiproxy provenance approach to uncovering the assembly of East Gondwana in Antarctica. *Geology*, 47, 645–649. <https://doi.org/10.1130/g45952.1>
- Müller, R. D., Cannon, J., Qin, X., Watson, R. J., Gurnis, M., Williams, S., et al. (2018). GPlates: Building a virtual earth through deep time. *Geochemistry, Geophysics, Geosystems*, 19, 2243–2261. <https://doi.org/10.1029/2018GC007584>
- Munroe, R. J., Sass, J. H., Milburn, G. T., Jaeger, J. C., & Tammemagi, H. Y. (1975). *Basic data for some recent Australian heat-flow measurements (75–567)*. Retrieved from <http://pubs.er.usgs.gov/publication/ofr75567>
- Neumann, N., Sandiford, M., & Foden, J. (2000). Regional geochemistry and continental heat flow: Implications for the origin of the south Australian heat flow anomaly. *Earth and Planetary Science Letters*, 183, 107–120. [https://doi.org/10.1016/S0012-821X\(00\)00268-5](https://doi.org/10.1016/S0012-821X(00)00268-5)
- Norwick, M. S., & Smith, M. A. (2001). Mapping the plate tectonic reconstruction of southern and southeastern Australia and implications for petroleum settings. *The APPEA Journal*, 41(1), 15–35. <https://doi.org/10.1071/AJ00001>
- Nyblade, A. A., Pollack, H. N., Jones, D. L., Podmore, F., & Mushayandebvu, M. (1990). Terrestrial heat flow in east and southern Africa. *Journal of Geophysical Research- Solid Earth*, 95, 17,371–17,384. <https://doi.org/10.1029/JB095iB11p17371>
- Overpeck, J. T., Otto-Bliesner, B. L., Miller, G. H., Muhs, D. R., Alley, R. B., & Kiehl, J. T. (2006). Paleo-climatic evidence for future ice-sheet instability and Rapid Sea-level rise. *Science*, 311, 1747–1750. <https://doi.org/10.1126/science.1115159>
- Pattyn, F. (2010). Antarctic subglacial conditions inferred from a hybrid ice sheet/ice stream model. *Earth and Planetary Science Letters*, 295, 451–461. <https://doi.org/10.1016/j.epsl.2010.04.025>
- Payne, J. L., Hand, M., & Barovich, K. M. (2007). Petrogenesis of ca 1.50 Ga granitic gneiss of the Coompana block: Filling the ‘magmatic gap’ of Mesoproterozoic Australia AU - Wade, B. P. *Australian Journal of Earth Sciences*, 54, 1089–1102. <https://doi.org/10.1080/08120090701615733>

- Payne, J. L., Hand, M., Barovich, K. M., Reid, A., & Evans, D. A. D. (2009). Correlations and reconstruction models for the 2500–1500 ma evolution of the Mawson continent. *Geological Society, London, Special Publications*, 323, 319–355. <https://doi.org/10.1144/sp323.16>
- Perry, H. K. C., Jaupart, C., Mareschal, J. C., & Bienfait, G. (2006). Crustal heat production in the Superior Province, Canadian shield, and in North America inferred from heat flow data. *Journal of Geophysical Research*, 111, B04401. <https://doi.org/10.1029/2005JB003893>
- Pittard, M. L., Galton-Fenzi, B. K., Roberts, J. L., & Watson, C. S. (2016). Organization of ice flow by localized regions of elevated geothermal heat flux. *Geophysical Research Letters*, 43, 3342–3350. <https://doi.org/10.1002/2016GL068436>
- Pollard, D., DeConto, R. M., & Nyblade, A. A. (2005). Sensitivity of Cenozoic Antarctic ice sheet variations to geothermal heat flux. *Global and Planetary Change*, 49, 63–74. <https://doi.org/10.1016/j.gloplacha.2005.05.003>
- Popov, Y. A., Pribnow, D. F., Sass, J. H., Williams, C. F., & Burkhardt, H. (1999). Characterization of rock thermal conductivity by high-resolution optical scanning. *Geothermics*, 28, 253–276.
- Pritchard, H. D., Ligtenberg, S. R. M., Fricker, H. A., Vaughan, D. G., van den Broeke, M. R., & Padman, L. (2012). Antarctic ice-sheet loss driven by basal melting of ice shelves. *Nature*, 484, 502. <https://doi.org/10.1038/nature10968>
- Purucker, M. (2013). Geothermal heat flux data set based on low resolution observations collected by the CHAMP satellite between 2000 and 2010, and produced from the MF-6 model following the technique described in Fox Maule et al. (2005). See <http://websrv.cs.umt.edu/isis/index.php>.
- Raimondo, T., Hand, M., & Collins, W. J. (2014). Compressional intracontinental Orogens: Ancient and modern perspectives. *Earth-Science Reviews*, 130, 128–153.
- Rankin, D. S., & Hyndman, R. D. (1971). Shallow water heat flow measurements in bras D'or Lake, Nova Scotia. *Canadian Journal of Earth Sciences*, 8, 96–101. <https://doi.org/10.1139/e71-006>
- Rignot, E., Velicogna, I., van den Broeke, M. R., Monaghan, A., & Lenaerts, J. T. M. (2011). Acceleration of the contribution of the Greenland and Antarctic ice sheets to sea level rise. *Geophysical Research Letters*, 38, L05503. <https://doi.org/10.1029/2011gl046583>
- Rimi, A. (1990). Geothermal gradients and heat flow trends in Morocco. *Geothermics*, 19, 443–454. [https://doi.org/10.1016/0375-6505\(90\)90057-I](https://doi.org/10.1016/0375-6505(90)90057-I)
- Roy, S., & Rao, R. U. M. (2000). Heat flow in the Indian shield. *Journal of Geophysical Research- Solid Earth*, 105, 25,587-25,604. <https://doi.org/10.1029/2000JB900257>
- Sandiford, M., McLaren, S., & Neumann, N. (2002). Long-term thermal consequences of the redistribution of heat-producing elements associated with large-scale granitic complexes. *Journal of Metamorphic Geology*, 20, 87–98. <https://doi.org/10.1046/j.0263-4929.2001.00359.x>
- Sass, J. H., & Lachenbruch, A. H. (1979). *Thermal Regime of the Australian Continental Crust*. London: Academic Press.
- Schroeder, D. M., Blankenship, D. D., Young, D. A., & Quartini, E. (2014). Evidence for elevated and spatially variable geothermal flux beneath the West Antarctic ice sheet. *Proceedings of the National Academy of Sciences*, 111, 9070–9072. <https://doi.org/10.1073/pnas.1405184111>
- Seroussi, H., Ivins, E. R., Wiens, D. A., & Bondzio, J. (2017). Influence of a West Antarctic mantle plume on ice sheet basal conditions. *Journal of Geophysical Research: Solid Earth*, 122, 7127–7155. <https://doi.org/10.1002/2017JB014423>
- Seroussi, H., Morlighem, M., Rignot, E., Khazendar, A., Larour, E., & Mouginot, J. (2017). Dependence of century-scale projections of the Greenland ice sheet on its thermal regime. *Journal of Glaciology*, 59, 1024–1034. <https://doi.org/10.3189/2013JoG13J054>
- Shapiro, N. M., & Ritzwoller, M. H. (2004). Inferring surface heat flux distributions guided by a global seismic model: Particular application to Antarctica. *Earth and Planetary Science Letters*, 223, 213–224. <https://doi.org/10.1016/j.epsl.2004.04.011>
- Siegent, M. J., & Dowdeswell, J. A. (1996). Spatial variations in heat at the base of the Antarctic ice sheet from analysis of the thermal regime above subglacial lakes. *Journal of Glaciology*, 42, 501–509. <https://doi.org/10.3189/S0022143000003488>
- Simkins, L. M., Anderson, J. B., Greenwood, S. L., Gonnermann, H. M., Prothro, L. O., Halberstadt, A. R. W., & DeConto, R. M. (2017). Anatomy of a meltwater drainage system beneath the ancestral East Antarctic ice sheet. *Nature Geoscience*, 10, 691. <https://doi.org/10.1038/ngeo3012>
- Smithies, R. H., Spaggiari, C. V., Kirkby, A. L., Wingate, M. T. D., & England, R. N. (2015a). Forrest Zone: geochemistry and petrogenesis. Retrieved from
- Smithies, R. H., Spaggiari, C. V., Kirkby, A. L., Wingate, M. T. D., & England, R. N. (2015b). Madura Province: geochemistry and petrogenesis. Retrieved from
- Spaggiari, C. V., Smithies, R. H., Kirkland, C. L., Wingate, M. T. D., England, R. N., & Lu, Y.-J. (2018). Buried but preserved: The Proterozoic Arubidby ophiolite, Madura Province, Western Australia. *Precambrian Research*, 317, 137–158. <https://doi.org/10.1016/j.precamres.2018.08.025>
- Szuman, I., Kalita, J. Z., & Ewertowski, M. W. (2018). The impact of geothermal heat flux on the last Scandinavian ice sheet over W Poland and E Germany. *Geografiska Annaler: Series A, Physical Geography*, 1–16. <https://doi.org/10.1080/04353676.2018.1524711>
- Szwilus, W., Afonso, J. C., Ebbing, J., & Mooney, W. D. (2019). Global crustal thickness and velocity structure from Geostatistical analysis of seismic data. *Journal of Geophysical Research: Solid Earth*, 124, 1626–1652. <https://doi.org/10.1029/2018jb016593>
- Totterdell, J. M., Blevin, J. E., Struckmeyer, H. I. M., Bradshaw, B. E., Colwell, J. B., & Kennard, J. M. (2000). A new sequence framework for the great Australian bight: Starting with a clean slate. *The APPEA Journal*, 40, 95–118. <https://doi.org/10.1071/AJ99007>
- Tucker, N. M., Payne, J. L., Clark, C., Hand, M., Taylor, R. J. M., Kylander-Clark, A. R. C., & Martin, L. (2017). Proterozoic reworking of Archean (Yilgarn) basement in the Bunger Hills, East Antarctica. *Precambrian Research*, 298, 16–38. <https://doi.org/10.1016/j.precamres.2017.05.013>
- Tulaczyk, S., Kamb, W. B., & Engelhardt, H. F. (2000). Basal mechanics of ice stream B, West Antarctica: 2. Undrained plastic bed model. *Journal of Geophysical Research- Solid Earth*, 105, 483–494. <https://doi.org/10.1029/1999JB900328>
- Van Liefferinge, B., & Pattyn, F. (2013). Using ice-flow models to evaluate potential sites of million year-old ice in Antarctica. *Climate of the Past*, 9, 2335–2345.
- Van Liefferinge, B., Pattyn, F., Cavitte, M. G. P., Karlsson, N. B., Young, D. A., Sutter, J., & Eisen, O. (2018). Promising oldest ice sites in East Antarctica based on thermodynamical modelling. *The Cryosphere*, 12, 2773–2787. <https://doi.org/10.5194/tc-12-2773-2018>
- Vila, M., Fernández, M., & Jiménez-Munt, I. (2010). Radiogenic heat production variability of some common lithological groups and its significance to lithospheric thermal modeling. *Tectonophysics*, 490, 152–164. <https://doi.org/10.1016/j.tecto.2010.05.003>
- Wade, B. P., Kelsey, D. E., Hand, M., & Barovich, K. M. (2008). The Musgrave Province: Stitching north, west and South Australia. *Precambrian Research*, 166, 370–386. <https://doi.org/10.1016/j.precamres.2007.05.007>
- Weber, R. D., Kirkby, A. L., & Gerner, E. J. (2011). Heat Flow Determinations for the Australian Continent: Release 3. Retrieved from
- White, L. T., Gibson, G. M., & Lister, G. S. (2013). A reassessment of paleogeographic reconstructions of eastern Gondwana: Bringing geology back into the equation. *Gondwana Research*, 24, 984–998. <https://doi.org/10.1016/j.gr.2013.06.009>

- Williams, M. A., Kelsey, D. E., Hand, M., Raimondo, T., Morrissey, L. J., Tucker, N. M., & Dutch, R. A. (2017). Further evidence for two metamorphic events in the Mawson continent. *Antarctic Science*, 30, 44–65. <https://doi.org/10.1017/S0954102017000451>
- Williams, S. E., Whittaker, J. M., Halpin, J. A., & Müller, R. D. (2019). Australian-Antarctic breakup and seafloor spreading: Balancing geological and geophysical constraints. *Earth-Science Reviews*, 188, 41–58. <https://doi.org/10.1016/j.earscirev.2018.10.011>
- Williams, S. E., Whittaker, J. M., & Müller, R. D. (2011). Full-fit, palinspastic reconstruction of the conjugate Australian-Antarctic margins. *Tectonics*, 30, TC002912. <https://doi.org/10.1029/2011tc002912>
- Winsborrow, M. C. M., Clark, C. D., & Stokes, C. R. (2010). What controls the location of ice streams? *Earth-Science Reviews*, 103, 45–59. <https://doi.org/10.1016/j.earscirev.2010.07.003>
- Wise, T., Pawley, M., & Dutch, R. A. (2018). Interpreted geology map of the eastern Coompana Province. Retrieved from Adelaide: Winsborrow, M. C. M., Clark, C. D., & Stokes, C. R. (2010). What controls the location of ice streams? *Earth-Science Reviews*, 103, 45–59. <https://doi.org/10.1016/j.earscirev.2010.07.003>
- Wyche, S., Lu, Y., & Wingate, M. T. D. (2019). Chapter 13 - evidence of hadean to Paleoarchean crust in the Youanmi and south west terranes, and eastern goldfields Superterrane of the Yilgarn craton, Western Australia. In M. J. van Kranendonk, V. C. Bennett, & J. E. Hoffmann (Eds.), *Earth's Oldest Rocks (2nd Edition)* (pp. 279–292). Elsevier.
- Zhang, Y. K. (1993). The thermal blanketing effect of sediments on the rate and amount of subsidence in sedimentary basins formed by extension. *Tectonophysics*, 218, 297–308. [https://doi.org/10.1016/0040-1951\(93\)90320-J](https://doi.org/10.1016/0040-1951(93)90320-J)